ELKHA : Jurnal Teknik Elektro, Vol. 15 No.2, October 2023, pp. 106 - 111
ISSN: 1858-1463 (print), 2580-6807 (online)

Rotor Speed Analysis of SMC-based IFOC for Low-Speed Induction Motor Control

Angga Wahyu Aditya[1*)], Ihsan[2)], Fachri Husaini[3)] and Faisal Faiiz Ramadhanu[4)]

[1, 2, 3, 4)] Department of Electrical Engineering, Politeknik Negeri Balikpapan, Indonesia
Corresponding Email: [*)] angga.wahyu@poltekba.ac.id

***Abstract* – The control of electric motors, particularly three-phase induction motors, has developed rapidly due to their application in industry. Indirect Field Oriented Control (IFOC) is one of the most widely used control systems due to its ease of application. IFOC controls a three-phase induction motor in the same way as a DC motor. However, IFOC requires a Sliding Mode Control (SMC) controller with Lyapunov stability theory to ensure robustness and stability. In exceptional conditions, such as low-speed settings, the SMC-based IFOC requires unique sets to operate with a steady-state error (Ess) at a speed response of less than 2%. Other parameters to be considered are rise time and electromagnetic torque response at low speeds. The addition of the boundary layer of the hyperbolic tangent function to a first-order SMC can increase induction motor (IM) control up to 175 rpm with a value of Ess = 1.96% compared to the saturation and signum functions, which are only capable of a reference speed of 300 rpm in no-load conditions with a value of Ess = 2% for the saturation function and 1.94% for the signum function. SMC with the hyperbolic tangent function boundary layer performs best under load conditions. The rising time value does not significantly differ under no-load or torque-load conditions between the SMC with the saturation, hyperbolic tangent function boundary layers and without the boundary layer. Adding a boundary layer with the hyperbolic tangent function can reduce ripple significantly compared to the saturation function under no-load or load conditions.**

Keywords: SMC, induction motor, IFOC, boundary layer, low speed control.

I. INTRODUCTION

The three-phase Induction Motor (IM) is a type of electric motor that is widely used in manufacturing, creative industries, and transportation [1]-[3]. IM has a simple but robust design, inexpensive, high efficiency, and easy maintenance [4]. However, IM has disadvantages such as high inrush current, poor starting torque, and difficulty control [5]. The weaknesses of IM have become a concern for researchers to develop solutions. Nowadays, along with the development of semiconductor technology, control devices such as inverters are one of the solutions used to overcome the weaknesses of IM [6]. Inverters can be equipped with controllers to enable the control of IM under various conditions while maintaining the robustness, stability, and performance of IM [7], [8].

The use of IM in transportation applications, such as electric cars, electric trains, and electric motorcycles, requires the control of IM at different speed ranges, including low, medium, and high speeds. A control system for induction motors that is robust and stable at high speeds has been developed through research on IM speed control using fuzzy sliding mode control combined with a reference adaptive system model without using a speed sensor and has undergone computer testing [9]. Similar research has focused on developing an advanced speed controller for IM using Indirect Field Oriented Control (IFOC). This research uses the Space Vector Pulse Width Modulation switching method to control the switching process in semiconductor devices [10]. The development of speed control methods for IM at high and medium speeds has focused on the type of methods used, such as conventional control (proportional-integral-derivative controller), particle swarm optimization, neural network, and fuzzy logic controllers [11]-[14].

Research on IM speed control using inverters is generally conducted at medium to nominal or high speed rather than low speed. Low-speed control is complicated to achieve [15]-[17]. This research focuses on controlling the IM speed at a low speed which has not been investigated yet by the previous researchers, to the author's best knowledge. An IFOC equipped with a first order Sliding Mode Control (SMC) is used for speed control.The chattering phenomenon in the first-order SMC is overcome using the boundary layer technique [18],19]. Considering the steady-state error and rise time in the speed response and the ripple in the electromagnetic torque response, the performance analysis is performed on the speed response and the electromagnetic torque under no-load and load conditions.

II. METHODOLOGY

The proposed system uses IFOC, which comes from IM's electrical and mechanical model. IFOC generally uses a conventional controller such as PID, and a model-free controller, such as a fuzzy controller, to get robustness and stability. The SMC purposed to bring stability and robustness simultaneously.

A. IFOC-IM

IFOC is one of the vector control methods widely used in IM. IFOC is more readily accepted by industry than Direct Field Oriented Control (DFOC) because the magnetic field in IM is measured by a particular sensor placed in the air gap. DFOC is considered impractical and only suitable for laboratory testing [20]. The IFOC equation is derived from the IM equation, so IFOC

Manuscript received 2023-07-06; revised 2023-09-16; accepted 2023-09-18

modeling is similar to IM. IFOC modeling consists of electrical and mechanical modeling [8]. Electrical modeling involves modeling the stator current and rotor flux in the dq rotating frame. The electrical modeling is expressed by state space equations [21]. The modeling of the rotor speed in IM is shown by Equation (1). Equation (2) shows that the IFOC modeling is focused on mechanical modeling, which consists of the IM speed modeling on the dq rotating frame, which is the focus of this research. At the same time, the electromagnetic torque equation in IFOC for IM is shown by Equation (3).

$$\frac{d\omega_r}{dt} = \frac{L_m}{jL_r}\left(\varphi_{rd} i_{qs} - \varphi_{rq} i_{ds}\right) - \frac{e_0}{j} \quad (1)$$

$$\frac{d\omega_r}{dt} = \frac{L_m}{jL_r}\left(\varphi_{rd} i_{qs}\right) - \frac{e_0}{j} \quad (2)$$

$$m_e = \frac{3}{2} P \frac{L_m}{L_r}\left(\varphi_{rd} i_{qs}\right) \quad (3)$$

where :
ω_r = rotor speed;
L_m = mutual inductance;
L_r = rotor inductance;
φ_{rd} = rotor flux in direct axis;
φ_{rq} = rotor flux in quadrature axis;
i_{ds} = stator current in direct axis;
i_{qs} = stator current in quadrature axis;
m_e = electromagnetic torque;
e_0 = torque load;
j = moment of inertia.

Based on Equations (2) and (3), the relationship between rotor speed and electromagnetic torque of IFOC modeling can be expressed in Equation (4).

$$\frac{d\omega_r}{dt} = \frac{2}{3Pj} m_e - \frac{e_0}{j} \quad (4)$$

B. SMC

The SMC is a controller that is classified as a model-based controller, so it requires system modeling to design the appropriate controller. The SMC in this study is shown in Equation (5). The equivalent Equation (U_{eq}) is obtained from the IFOC modeling for IM. SMC can ensure the stability and robustness of the system by using the Lyapunov stability theory in the design of the equivalent Equation. The first-order robustness of SMC is obtained by the signum function in U_n.

First-order SMC has the disadvantage of chattering [22]-[24]. This phenomenon is very detrimental to the IM as it consumes large amounts of energy and generates excessive heat, which can damage the IM components. This phenomenon can be overcome by increasing the order of the SMC or by providing a boundary layer in the U_n equation. A simple method is to add a boundary layer using the saturation or hyperbolic tangent functions, as shown in Figures 1 and 2 [18].

In this study, the first-order SMC equation with the signum function in IFOC for IM is designed to control the rotor speed, as shown in Equation (7). The implementation of the boundary layer using saturation and hyperbolic tangent functions causes the U_n equation to change to Equations (8) and (9) with α_{ω_r}, β_{ω_r}, γ_{lyr} and δ_{lyr} is a positive constant.

$$U_{eq}(m_e) = \frac{3}{2} jP(\omega_r{}^* + \frac{e_o}{j}) \quad (5)$$

$$U_n = \alpha_{\omega_r} S_{\omega_r}(e_{\omega_r}) + \beta_{\omega_r}\, sign\,(S_{\omega_r}(e_{\omega_r})) \quad (6)$$

$$U_C = U_{eq} + U_n \quad (7)$$

$$U_n = \alpha_{\omega_r} S_{\omega_r}(e_{\omega_r}) + \gamma_{lyr}\, sat\,(S_{\omega_r}(e_{\omega_r})) \quad (8)$$

$$U_n = \alpha_{\omega_r} S_{\omega_r}(e_{\omega_r}) + \delta_{lyr}\, tanh\,(S_{\omega_r}(e_{\omega_r})) \quad (9)$$

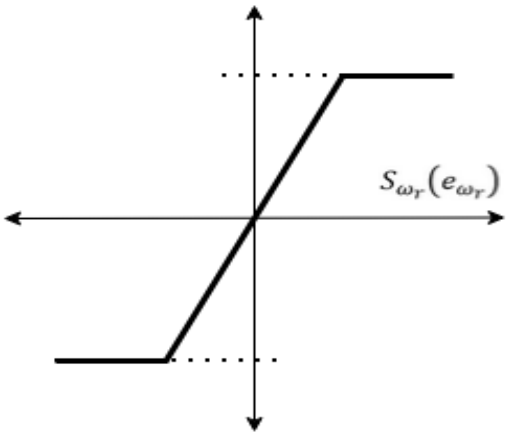

Figure 1. Boundary layer using saturation function

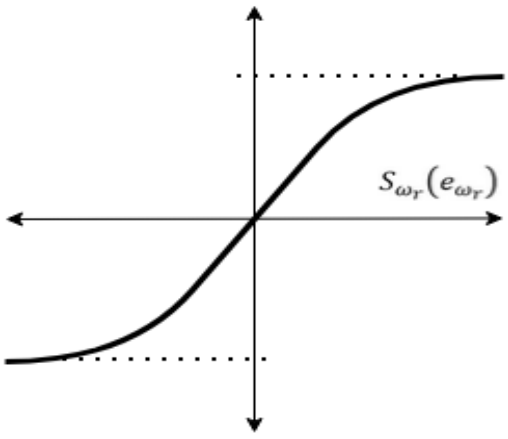

Figure 2. Boundary layer using hyperbolic tangent function

III. RESULTS AND DISCUSSION

Electromagnetic speed and torque response data were collected through computer testing using MATLAB Simulink software. The tests were carried out with two types of speed reference. The first stage is testing with a speed reference of 400 rpm for 2 seconds; then the speed reference is changed to 300 rpm until the fourth second, then the speed reference is increased by 50 rpm to 350

rpm for 2 seconds, then the speed reference is reduced to 200 rpm for two seconds and finally reduced to 100 rpm at the eighth second. The load in this type changes from 0.5 Nm to 1.5 Nm. The next type of test is a speed response test using a constant speed reference with constant loads of 0 (no-load condition), 0.5, 1, and 1.5 Nm. Figure 3 shows the speed response of the MI in the first type of test with the results of the steady-state error analysis shown in Table 1.

Applying a boundary layer to a first-order SMC for low-speed IM control using IFOC significantly reduced Ess. At a reference speed of 400 rpm, the saturation and hyperbolic tangent functions can reduce the Ess value by up to 0.61%. However, at a reference speed of 300 rpm, the saturation function causes an increase in Ess that exceeds the tolerance limit of 2%. The load test with a torque load of 1 Nm shows that only the signum and hyperbolic tangent functions can produce Ess values below the tolerance limit of 2%, as shown in Table 1. When tested at a shallow reference speed (200 rpm), the tanh function () can provide Ess values below the 2% tolerance with a torque load of up to 1.5 Nm. On the other hand, the signum and saturation functions require parameter adjustments through artificial intelligence to obtain optimum values concerning Ess tolerances below 2%. The determination of the parameters of the first-order SMC constants and the boundary layer in the computational test was done intuitively.

Table 1. Ess Analysis in Variable Reference Speed

Reference Speed (rpm)	Torque Load (Nm)	*Error Steady-State (%)*		
		Sign()	***Sat()***	***Tanh()***
400	0	1.45	1.36	0.84
300	0	1.94	2.02	1.17
	1	1.93	2.53	1.15
350	1	1.59	2.10	0.97
	0.5	1.59	1.89	0.97
200	0.5	2.91	3.66	1.72
	1.5	2.91	4.50	1.72
100	1.5	5.80	9.49	3.42
	0	5.83	6.81	3.43

In the second test, the speed was constant at 50 – 400 rpm with a range of 25 rpm. The torque load in this test is given when MI is run. The torque load is 0 Nm (no-load condition), 0.5, 1, and 1.5 Nm. Loading is intended to determine the performance of the SMC controller with the signum, saturation, and hyperbolic tangent functions. The analysis was performed at Ess and rising time. The no-load condition produces an Ess value of 11.69% in the signum function, 13.21% in the saturation function, and 6.97% in the hyperbolic tangent function at a reference speed of 50 rpm. These results indicate that the first-order SMC, whether with a boundary layer or not, cannot perform IFOC-based IM settings because the Ess value exceeds the tolerance limit of 2%. The Ess value that meets the 2% tolerance limit at no-load conditions for the signum function is at a speed reference of 300 rpm (Ess = 1.94%), the saturation function is 300 rpm (Ess = 2%), and the hyperbolic tangent function is 175 rpm which shown in Figure 4(a). Giving a torque load of 0.5 Nm shows a change in reference speed that can be accommodated by a first-order SMC with a boundary layer of the saturation function to 350 rpm (Ess = 1.88%) but does not affect the signum and hyperbolic tangent functions. The same results were obtained when the torque load was increased to 1 Nm and 1.5 Nm. The SMC with the signum function and the SMC with the hyperbolic tangent function boundary layer were able to maintain an Ess tolerance of 2% with reference speeds of 300 rpm and 175 rpm. The SMC uses a boundary layer with the saturation function at a reference speed of 375 rpm for a torque load of 1 Nm and 400 rpm for a torque load of 1.5 Nm. In general, the Ess value for both no-load and load conditions will experience an exponential decrease, as shown in Figures 4(a), 5(a), 6(a), and 7(a). The Rising time value at no torque load and 0.5, 1, and 1.5 Nm torque load does not have a significant difference either at the SMC with the signum function, with the saturation and hyperbolic tangent boundary layers as shown in Figure 4(b), 5 (b), 6(b) and 7(b).

Electromagnetic torque analysis is carried out on the changes in electromagnetic torque ripple as torque loads are applied and removed. It is to determine the performance of the SMC on the IFOC system for IM using the signum, saturation, and hyperbolic tangent functions. Under no-load conditions with a reference speed of 400 rpm, providing a boundary layer with the saturation function can reduce the electromagnetic torque ripple by 5.66%. In contrast, the hyperbolic tangent function can reduce it by 40.47%. At a load of 1 Nm in the third second with a reference speed of 300 rpm, as shown in Figure 8, there is a 21.14% increase in the electromagnetic torque ripple with the saturation function. In contrast, the hyperbolic tangent function reduces the electromagnetic torque ripple by 29.14%. A load of 1 Nm results in an increase in the electromagnetic torque ripple. The growth is 0.17% for the signum function, 28.64% for the saturation function, and 19.24% for the hyperbolic tangent function. At a reference speed of 350 rpm, with a reduced torque load of 0.5 Nm, there is an increase in the electromagnetic torque ripple of 18.48% in the saturation function compared to the signum function. Meanwhile, in the hyperbolic tangent function, the electromagnetic torque ripple has decreased by 39.72%. The increase in ripple in this condition is 8.12% for the signum function, 5.71% for the saturation function, and 8.47% for the hyperbolic tangent function. The increase in the torque load, which reaches 1.5 Nm in the seventh second, causes an increase in the electromagnetic torque ripple of 43.45% for the saturation function compared to the signum function. In contrast, the hyperbolic tangent function has a 29.28% decrease. Figure 9 shows the reduction in electromagnetic torque ripple as the torque load changes from 1.5 Nm to 0 Nm. In this condition, the signum and hyperbolic tangent functions do not experience significant changes, but the saturation function experiences a 29.66% decrease in electromagnetic torque ripple.

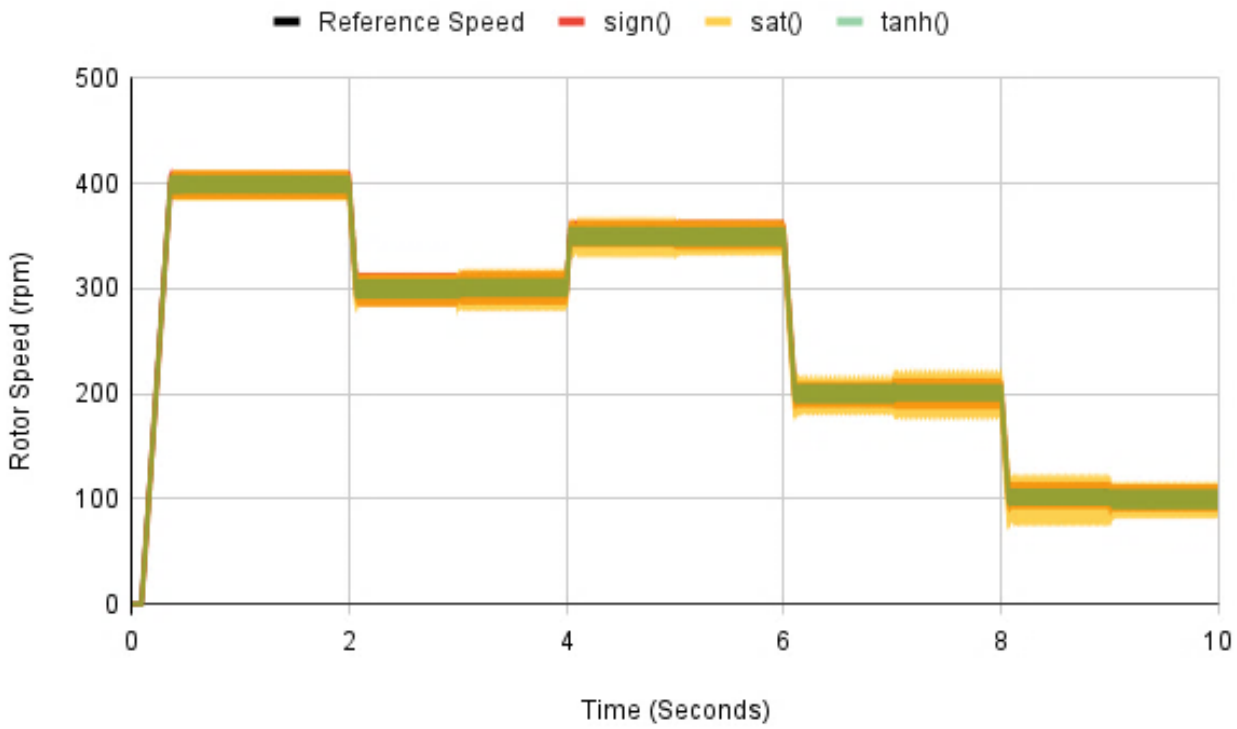

Figure 3. Rotor speed response of IM in variable reference speed

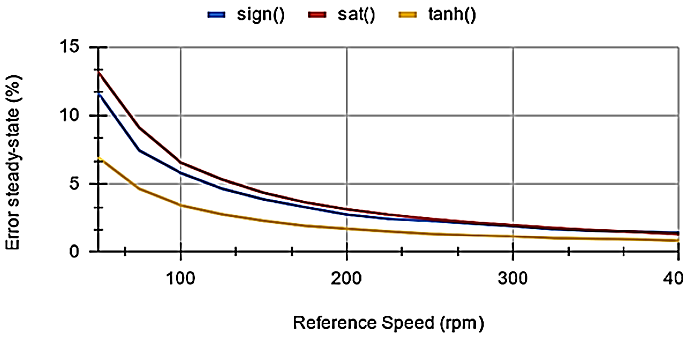

(a)

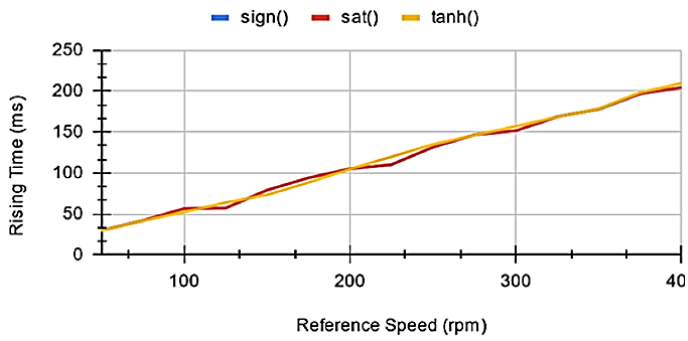

(b)

Figure 4. (a) Ess (b) Rising time of IM in no-load condition

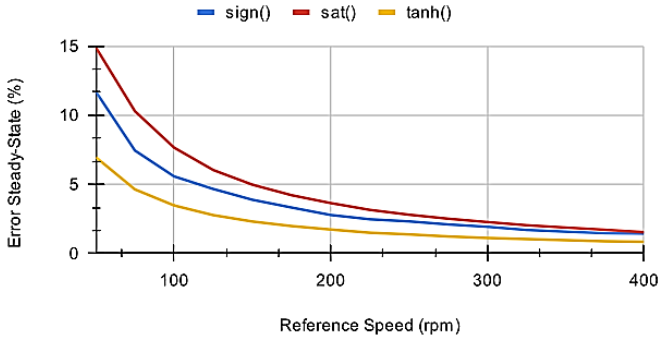

(a)

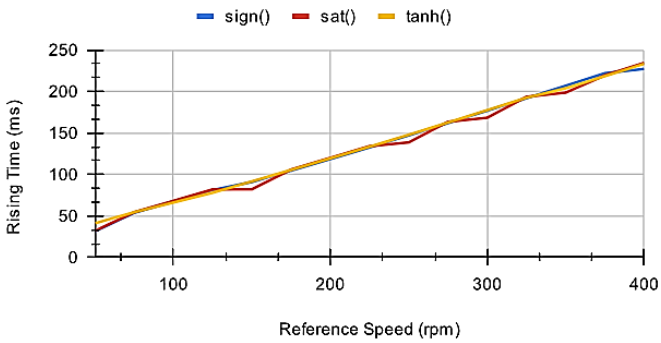

(b)

Figure 5. (a) Ess (b) Rising time of IM with torque load = 0.5 Nm

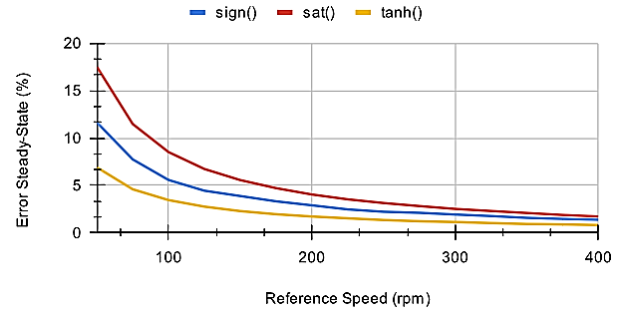

(a)

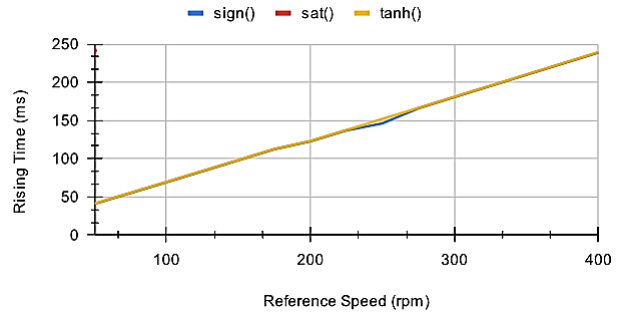

(b)

Figure 6. (a) Ess (b) Rising time of IM with torque load = 1 Nm

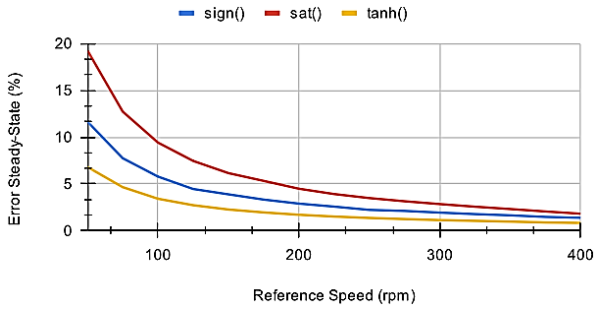

(a)

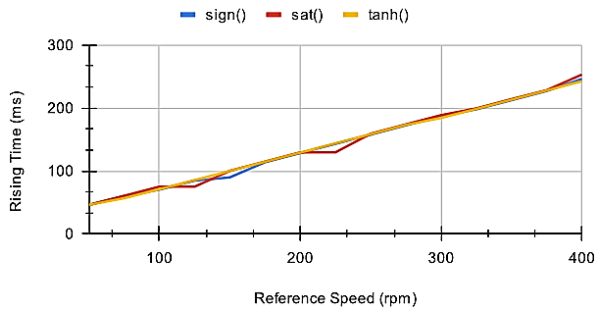

(b)

Figure 7. (a) Ess (b) Rising time of IM with torque load = 1.5 Nm

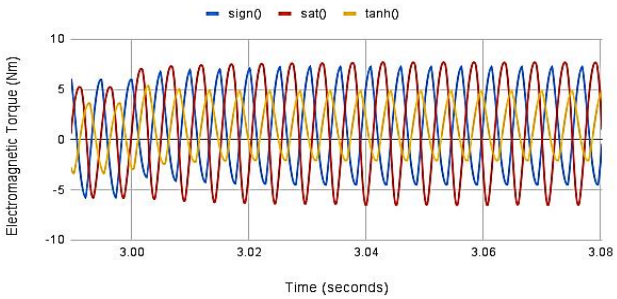

Figure 8. Electromagnetic torque response at 1 Nm of torque load increase

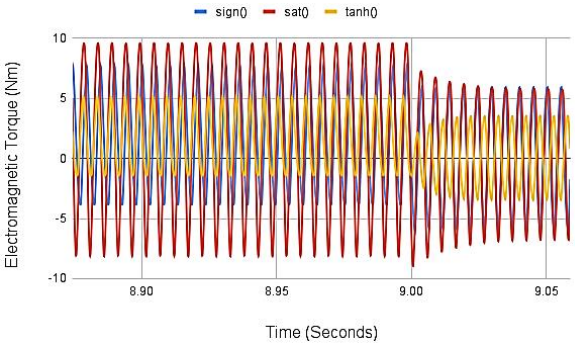

Figure 9. Electromagnetic torque response at 1.5 Nm of torque load decrease

IV. CONCLUSION

IFOC-based IM settings with low-speed first-order SMC require a chattering phenomenon regulation mechanism. Giving a boundary layer to a first-order SMC to reduce the Ess value with the saturation function is not fully effective because the saturation function cannot compensate for chattering phenomena under load conditions. The development of the boundary layer with the hyperbolic tangent function can reduce the Ess value in first-order SMC with the signum function up to 39.75% at no-load conditions, 39.72% at 0.5 Nm torque load, 40.06% at 1 Nm torque load and 40.49% at torque load 1.5Nm. The rising time characteristics of the first-order SMC with the signum function and the SMC with the boundary layer functions saturation and tanh have no significant difference under no-load or load conditions. In addition, implementing the boundary layer with the hyperbolic tangent function can reduce electromagnetic torque ripples, which cannot be done by the saturation function.

ACKNOWLEDGMENT

The authors would like to thank the General Directorate of Vocational Education - Ministry of Education, Culture, Research and Technology. This research was funded by the Basic Research Scheme with the scope of PDP Research in 2023 with main contract number 181/SPK/D.D4/PPK.01.APTV/VI/2023 and derivative contract number 02/PL32.13/SPK-LT/2023. The authors would like to thank the Department of Electrical Engineering and the Centre for Research and Community Service of Balikpapan State Polytechnic.

REFERENCES

[1] M. Drakaki, Y. L. Karnavas, P. Tzionas, and I. D. Chasiotis, "Recent Developments Towards Industry 4.0 Oriented Predictive Maintenance in Induction Motors," *Procedia Comput. Sci.*, vol. 180, pp. 943–949, Jan. 2021.

[2] A. W. Aditya, I. Ihsan, R. M. Utomo, and H. Hilmansyah, "Evaluasi Motor Listrik Sebagai Penggerak Mobil Listrik," *JRST (Jurnal Riset Sains dan Teknologi)*, vol. 3, no. 2, pp. 55-59, Sep. 2019.

[3] Y. Dhayaneswaran and L. Ashok Kumar, "A study on current characteristics of induction motor while operating

at its base frequency in textile industry," *Energy*, vol. 74, no. C, pp. 340–345, Sep. 2014.

[4] S. J. Rind, Y. Ren, Y. Hu, J. Wang, and L. Jiang, "Configurations and control of traction motors for electric vehicles: A review," *Chinese J. Electr. Eng.*, vol. 3, no. 3, pp. 1–17, Dec. 2017.

[5] S. Vadi, R. Bayindir, Y. Toplar, and I. Colak, "Induction motor control system with a Programmable Logic Controller (PLC) and Profibus communication for industrial plants — An experimental setup," *ISA Trans.*, vol. 122, pp. 459–471, Mar. 2022.

[6] Y. Kumsuwan, W. Srirattanawichaikul, and S. Premrudeepreechacharn, "A simple voltage and frequency control of VSI-inverter-fed self-excited induction generator drive," *2009 ICCAS-SICE*, 2009. https://ieeexplore.ieee.org/document/5335133 (accessed Jun. 17, 2023).

[7] A. Wahyu Aditya, M. Rizani Rusli, B. Praharsena, E. Purwanto, D. Cahya Happyanto, and B. Sumantri, "The Performance of FOSMC and Boundary - SMC in Speed Controller and Current Regulator for IFOC-Based Induction Motor Drive," *Proc. - 2018 Int. Semin. Appl. Technol. Inf. Commun. Creat. Technol. Hum. Life, iSemantic 2018*, pp. 139–144, Nov. 2018.

[8] D. C. Happyanto, A. W. Aditya, and B. Sumantri, "Boundary–Layer Effect in Robust Sliding Mode Control for Indirect Field Oriented Control of 3-Phase Induction Motor," *Int. J. Electr. Eng. Informatics*, vol. 12, no. 2, pp. 188–204, Jun. 2020.

[9] D. Fereka, M. Zerikat, and A. Belaidi, "MRAS Sensorless Speed Control of an Induction Motor Drive based on Fuzzy Sliding Mode Control," *2018 7th Int. Conf. Syst. Control. ICSC 2018*, pp. 230–236, Dec. 2018.

[10] G. Arpit, H. P. Singh, and K. Pandey, "Advance speed control of three phase induction motor using field oriented control method," *Mater. Today Proc.*, vol. 80, pp. 1981–1985, Jan. 2023.

[11] K. Kecepatan Motor Induksi *et al.*, "Kendali Kecepatan Motor Induksi 3 Fase Berbasis Particle Swarm Optimization (PSO)," *ELKOMIKA J. Tek. Energi Elektr. Tek. Telekomun. Tek. Elektron.*, vol. 8, no. 3, p. 477, Aug. 2020.

[12] H. Sathishkumar and S. S. Parthasarathy, "A novel neural network intelligent controller for vector controlled induction motor drive," *Energy Procedia*, vol. 138, pp. 692–697, Oct. 2017.

[13] H. Sathishkumar and S. S. Parthasarathy, "A novel neuro-fuzzy controller for vector controlled induction motor drive," *Energy Procedia*, vol. 138, pp. 698–703, Oct. 2017.

[14] J. K. Jain, S. Ghosh, S. Maity, and P. Dworak, "PI controller design for indirect vector controlled induction motor: A decoupling approach," *ISA Trans.*, vol. 70, pp. 378–388, Sep. 2017.

[15] Y. A. Zorgani, M. Jouili, Y. Koubaa, and M. Boussak, "A Very-Low-Speed Sensorless Control Induction Motor Drive with Online Rotor Resistance Tuning by Using MRAS Scheme," *Power Electron. Drives*, vol. 4, no. 1, pp. 125–140, Jun. 2019.

[16] E. Purwanto, I. Ferdiansyah, S. D. Nugraha, and O. A. Qudsi, "The Effect of ANFIS Controller on The Performance of Induction Motor Drives in Low-Speed Operation Based on IFOC," *Int. J. Adv. Sci. Eng. Inf. Technol.*, vol. 11, no. 2, p. 440, Apr. 2021.

[17] Y. Zahraoui, M. Akherraz, C. Fahassa, and S. Elbadaoui, "Induction Motor DTC Performance Improvement by Reducing Flux and Torque Ripples in Low Speed," *J. Robot. Control*, vol. 3, no. 1, pp. 93–100, Jan. 2022.

[18] D. C. Happyanto and A. W. Aditya, "Chattering reduction effect on power efficiency of IFOC based induction motor," *J. INFOTEL*, vol. 14, no. 2, pp. 154–160, May 2022.

[19] E. Taheri, M. H. Ferdowsi, and M. Danesh, "Design Boundary Layer Thickness and Switching Gain in SMC Algorithm for AUV Motion Control," *Robotica*, vol. 37, no. 10, pp. 1785–1803, Oct. 2019.

[20] H. Abu-Rub, A. Iqbal, and J. Guzinski, *High Performance Control of AC Drices With MATLAB/Simulink Models*, Second Edi. John Wiley & Sons Ltd, 2021.

[21] A. Aditya, A. W. Aditya, I. Ihsan, R. M. Utomo, and H. Hilmansyah, "Pemodelan State Space Motor Induksi Tiga Fasa Sebagai Penggerak Mobil Listrik," *J. Teknol.*, vol. 12, no. 1, pp. 39–48, Feb. 2020.

[22] S. Kapat, "Chattering-Free Event-Trigger Fast Recovery Stable Digital Sliding Mode Control in DC-DC Converters," *Conf. Proc. - IEEE Appl. Power Electron. Conf. Expo. - APEC*, pp. 1248–1252, 2022.

[23] T. T. Tran and V. H. Nguyen, "A Novel Design of Chattering-free Sliding Mode Control for a Nonlinear Dynamic System," *2021 4th Int. Conf. Robot. Control Autom. Eng. RCAE 2021*, pp. 213–217, 2021.

[24] R. Ramezanzadeh, S. M. H. Baygi, J. Farzaneh, and A. Karsaz, "Chattering-free blood glucose level control based on ANFIS," *IEEE Int. Conf. Fuzzy Syst.*, Aug. 2017.